

Chiral anomaly and ultrahigh mobility in crystalline HfTe₅Huichao Wang,^{1,2} Chao-Kai Li,^{1,2} Haiwen Liu,^{1,2,3} Jiaqiang Yan,^{4,5} Junfeng Wang,⁶ Jun Liu,⁷ Ziquan Lin,⁶ Yanan Li,^{1,2} Yong Wang,⁷ Liang Li,⁶ David Mandrus,^{4,5} X. C. Xie,^{1,2} Ji Feng,^{1,2} and Jian Wang^{1,2,*}¹*International Center for Quantum Materials, School of Physics, Peking University, Beijing 100871, China*²*Collaborative Innovation Center of Quantum Matter, Beijing 100871, China*³*Center for Advanced Quantum Studies, Department of Physics, Beijing Normal University, Beijing, 100875, China*⁴*Department of Materials Science and Engineering, University of Tennessee, Knoxville, Tennessee 37996, USA*⁵*Materials Science and Technology Division, Oak Ridge National Laboratory, Oak Ridge, Tennessee 37831, USA*⁶*Wuhan National High Magnetic Field Center, Huazhong University of Science and Technology, Wuhan 430074, China*⁷*Center of Electron Microscopy, State Key Laboratory of Silicon Materials, Department of Materials Science and Engineering, Zhejiang University, Hangzhou 310027, China*

(Received 30 December 2015; revised manuscript received 24 March 2016; published 19 April 2016)

HfTe₅ is predicted to be a promising platform for studying topological phases. Here through an electrical transport study, we present an observation of chiral anomaly and ultrahigh mobility in HfTe₅ crystals. Negative magnetoresistivity in HfTe₅ is observed when the external magnetic and electrical fields are parallel ($\mathbf{B} // \mathbf{E}$) and quickly disappears once \mathbf{B} deviates from the direction of \mathbf{E} . Quantitative fitting further confirms the chiral anomaly as the underlying physics. Moreover, by analyzing the conductivity tensors of longitudinal and Hall traces, ultrahigh mobility and ultralow carrier density are revealed in HfTe₅, which paves the way for potential electronic applications.

DOI: [10.1103/PhysRevB.93.165127](https://doi.org/10.1103/PhysRevB.93.165127)**I. INTRODUCTION**

Chiral anomaly is a quantum anomaly phenomenon that breaks the chiral symmetry and leads to the nonconservation of chiral current [1,2]. This anomaly was proposed to be observed in a lattice system in 1983 [3]. Recently, the study of Weyl fermions pushes forward the realization of chiral anomaly in crystals [4–6]. In Dirac/Weyl semimetals, the axial current is nonconserved due to the chiral anomaly, and further leads to charge pumping effect between the Weyl nodes with opposite chirality. This anomaly effect is suggested to give rise to negative magnetoresistivity when the magnetic and electrical fields are parallel ($\mathbf{B} // \mathbf{E}$) [4]. Related experimental evidences have been intensively pursued in various condensed matter systems [7–20].

HfTe₅ is a layered material with a van der Waals coupling between the individual layers. It crystallizes in an orthorhombic structure with the space group *Cmcm* [21]. The trigonal prismatic chains of “HfTe₃” along the *a* axis are linked along the *c* axis via parallel zigzag chains of “Te₂”, forming a two-dimensional (2D) sheet of HfTe₅ in the *a-c* plane. The sheets of HfTe₅ stack along the *b* axis. HfTe₅ has been previously studied for its resistivity anomaly [22,23], thermoelectric properties [24], and quantum oscillations [25,26]. Previous *ab initio* study has predicted that HfTe₅ and ZrTe₅ crystals are located near the phase boundary between weak and strong topological insulators [27]. Successive ARPES results reveal that ZrTe₅ is a three-dimensional Dirac semimetal [13]. Moreover, recent experimental investigations have shown that ZrTe₅ possesses many peculiar features, such as the $B^{1/2}$ dependence of inter-Landau-level resonance [28,29] and nontrivial Berry phase [29], which confirm the existence of Dirac fermions in the system. Particularly, the chiral anomaly is observed in magnetotransport measurements

of ZrTe₅ [13]. However, theoretically predicted topological material HfTe₅ has rarely been confirmed and studied experimentally.

Here we present electrical transport evidence for the chiral anomaly and the ultrahigh mobility in HfTe₅ crystals. Specifically, anomalous negative magnetoresistivity is observed when the magnetic field \mathbf{B} is aligned along the direction of electrical field \mathbf{E} . It is quite sensitive to the orientation of \mathbf{B} relative to \mathbf{E} and disappears rapidly when \mathbf{B} deviates from \mathbf{E} . Quantitative analyses suggest the negative magnetoresistivity originates from the chiral anomaly. Moreover, Hall trace of HfTe₅ crystal is studied. By analyzing both the longitudinal and Hall conductivities in a two-carrier model, we find HfTe₅ has ultrahigh mobility and ultralow carrier density especially at low temperatures. The Hall trace also shows that in our HfTe₅ samples only hole type carriers contribute to the Fermi surface, which is consistent with the previously calculated band structure of HfTe₅ [27].

II. RESULTS AND DISCUSSION

HfTe₅ crystals were grown out of Te flux using a Canfield crucible set (CCS) [30]. The self-flux growth yields high quality crystals as in the case of WTe₂ [31]. Hf pieces and Te shots in an atomic ratio of 1:99 were loaded into the CCS and then sealed in a silica ampoule under vacuum. The sealed ampoule was heated to 800 °C and kept for 8 h to homogenize the melt, furnace cooled to 600 °C, and then cooled down to 460 °C in 48 h. HfTe₅ crystals were isolated from Te flux by centrifuging once the furnace temperature reached 460 °C. Typical HfTe₅ samples are about 10–20 mm long with the other two dimensions in the range of 0.01–0.6 mm. The longest direction is always along the crystallographic *a* axis.

We use a FEI TITAN Cs-corrected cross-sectional STEM operating at 200 kV to examine the HfTe₅ crystal. As shown in Fig. 1(a), the atomic layer-by-layer high angle annular dark

*Corresponding author: jianwangphysics@pku.edu.cn

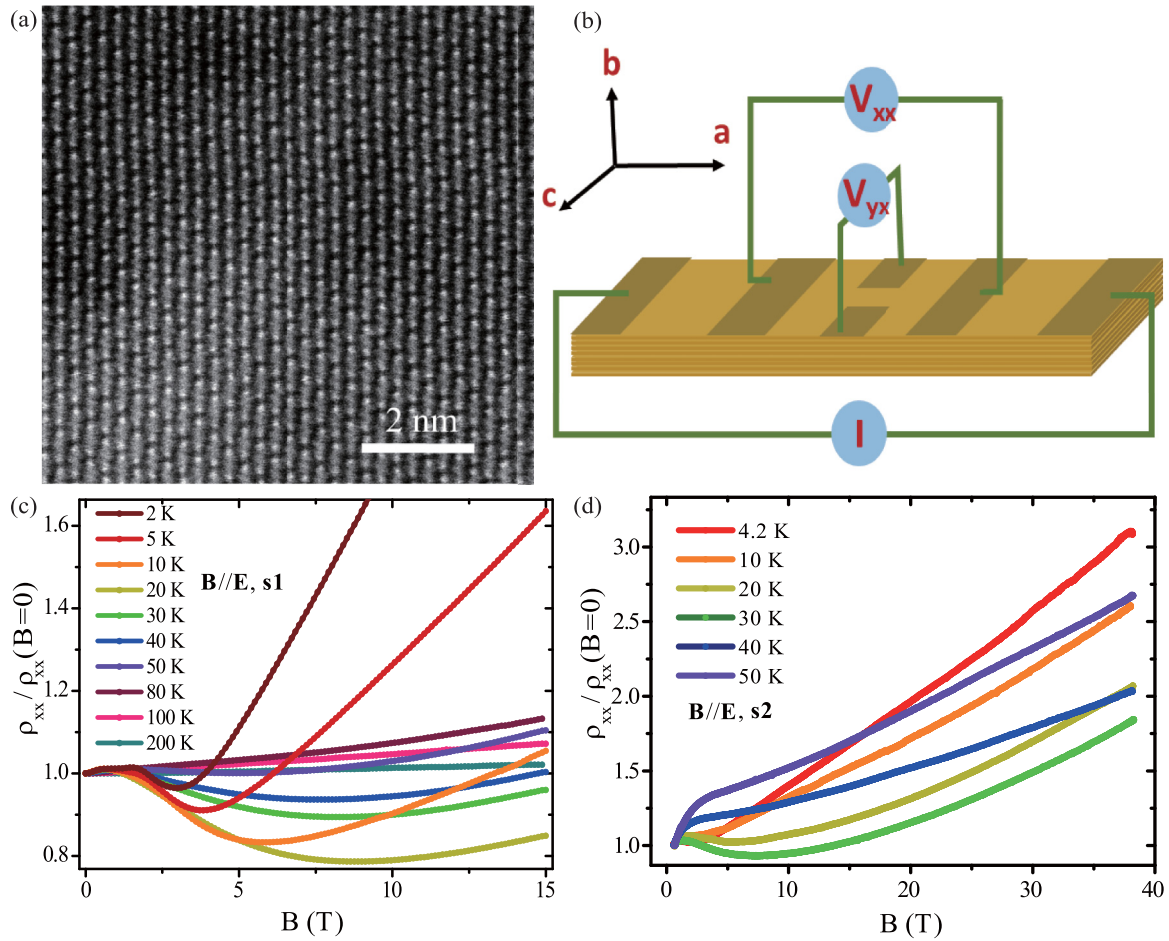


FIG. 1. (a) HAADF STEM image of a typical HfTe_5 crystal. Scale bar represents 2 nm. (b) A schematic structure for the electrical transport measurements of HfTe_5 . Standard four (six)-probe method is used for the resistivity (resistivity and Hall trace) measurement. (c) Temperature dependence of the normalized magnetoresistivity in HfTe_5 sample 1 (s1) when $\mathbf{B} // \mathbf{E}$, s1. (d) Normalized magnetoresistivity of sample 2 (s2) extended to 38 T at selected temperatures with $\mathbf{B} // \mathbf{E}$.

field (HAADF) STEM image manifests a high-quality nature of the HfTe_5 crystal. Electrical transport measurements are mainly conducted in a 16T-Physical Property Measurement System (PPMS-16T) from Quantum Design. High magnetic field study extended to 38 T is performed in the Wuhan National High Magnetic Field Center. A standard four (six)-probe method is used for measuring resistivity (resistivity and Hall trace). Electrical contacts were made by using 25- μm -diameter Au wires bonded to the crystal with silver paint. A schema of the measurement configuration is shown in Fig. 1(b). The external electrical field \mathbf{E} is always along the a axis in our work. The sample is rotated to form a different orientation relative to the magnetic field. Tens of samples from the same batch are studied and typical results are shown in the main text.

We explore the chiral anomaly of HfTe_5 in the measurement configuration when both magnetic and electrical fields are aligned along the a axis. Figure 1(c) shows the normalized magnetoresistivity of sample 1 (s1) at selected temperatures when $\mathbf{B} // \mathbf{E}$. In the very weak \mathbf{B} around $\mathbf{B} = 0$, the sample shows positive magnetoresistivity signaling weak antilocalization effect induced by the strong spin-orbit coupling.

Surprisingly, an anomalous negative magnetoresistivity is observed at low temperatures, which almost disappears at 50 K. At the large \mathbf{B} regime, the magnetoresistivity becomes positive which may be due to the electron-electron interaction or the misalignment of excitation current with external magnetic field. With similar results to s1 below 15 T, s2 is further measured in pulsed magnetic field up to 38 T with $\mathbf{B} // \mathbf{E}$, as shown in Fig. 1(d). At the high magnetic field above 15 T, s2 shows positive magnetoresistivity without any oscillation. Specially, linear magnetoresistivity is observed at 4.2 K in a large magnetic field regime, similar to the observation in the Dirac semimetal Cd_3As_2 system [9,32,33].

For chiral anomaly induced negative magnetoresistivity, it is predicted to be most evident when $\mathbf{B} // \mathbf{E}$. To test the property of our measured negative magnetoresistivity, we rotate s1 in the a - b plane at 2 K. When the b axis of s1 is aligned to the magnetic field direction ($\theta = 0^\circ$), i.e., \mathbf{B} is perpendicular to \mathbf{E} , the magnetoresistivity is always positive and saturated at high magnetic fields [Fig. 2(a)]. With the sample tilted to a larger θ , the magnetoresistivity becomes smaller and decreases abruptly around $\theta = 90^\circ$. More detailed measurement results around $\theta = 90^\circ$ are shown in Fig. 2(b).

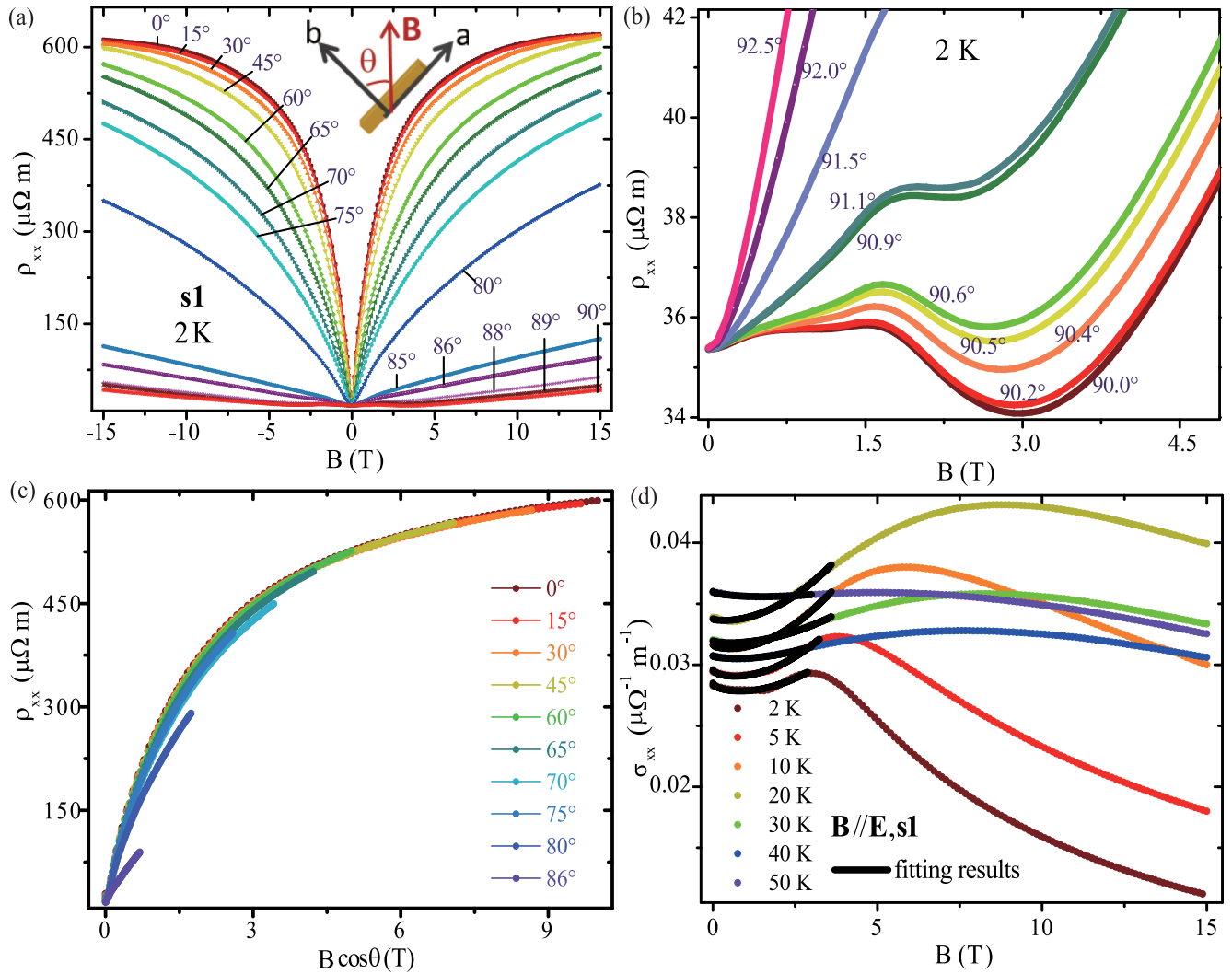


FIG. 2. (a) Magnetoresistivity ρ_{xx} vs \mathbf{B} at selected angles θ when $s1$ is rotated in the a - b plane. The magnetic field is along b axis ($\mathbf{B} \perp \mathbf{E}$) for $\theta = 0^\circ$ and along a axis ($\mathbf{B} // \mathbf{E}$) for $\theta = 90^\circ$. (b) Anomalous negative magnetoresistivity in $s1$ when the external magnetic and electrical fields are nearly parallel. (c) Magnetoresistivity vs the perpendicular component of magnetic field $\mathbf{B} \cos \theta$. Results at small θ indicate a quasi-two-dimensional nature. (d) Quantitative fitting for the magnetoconductivity of $s1$ at different temperatures from 0 to about 3 T when $\mathbf{B} // \mathbf{E}$. Dots are experimental data and black lines are fitting results with Eq. (1).

The negative magnetoresistivity is most evident when $\mathbf{B} // \mathbf{E}$ and can survive only if the relative orientation of \mathbf{B} and \mathbf{E} is smaller than 1° . Magnetoresistivity of $s1$ below 10 T as a function of the perpendicular field component $\mathbf{B} \cos \theta$ is shown in Fig. 2(c). We find that the results for small θ ($< 65^\circ$) can be perfectly collapsed onto one single curve, suggesting a quasi-two-dimensional feature. However, the $\rho_{xx}(\mathbf{B})$ curves obtained at large θ ($65^\circ < \theta < 90^\circ$) deviate from the scaling. When θ is close to 90° ($\mathbf{B} // \mathbf{E}$), the deviation becomes quite apparent, indicating other certain underlying effects.

The study in high magnetic field up to 38 T shows that the negative magnetoresistivity is not a part of Shubnikov-de Haas (SdH) oscillation. In addition, the corresponding magnetic field for resistivity minimum is shifting at different temperatures, which is also inconsistent with the SdH behavior. On the other hand, as the angle-dependent results shown

in Fig. 2(b), the negative magnetoresistivity can only be observed when \mathbf{B} is aligned to within 1° of the direction of \mathbf{E} . Thus, the weak localization effect which is not so sensitive to the direction of \mathbf{B} with respect to \mathbf{E} can be excluded. All these peculiar features in our observation point to a highly possible mechanism, the chiral anomaly. For further confirmation, quantitative analyses are carried out by fitting the experimental results in Fig. 2(d) with a simplified semiclassical formula [7]

$$\sigma_{xx} = (\sigma_0 - a\sqrt{B})(1 + C_w B^2), \quad (1)$$

where the first term is related to a weak antilocalization correction with coefficient $a > 0$ and the second term is associated with the chiral anomaly. σ_0 is the zero field conductivity and C_w is a positive parameter. Black lines in Fig. 2(d) are produced by Eq. (1). The nice match between theoretical fitting and experimental results from 0 to about 3 T

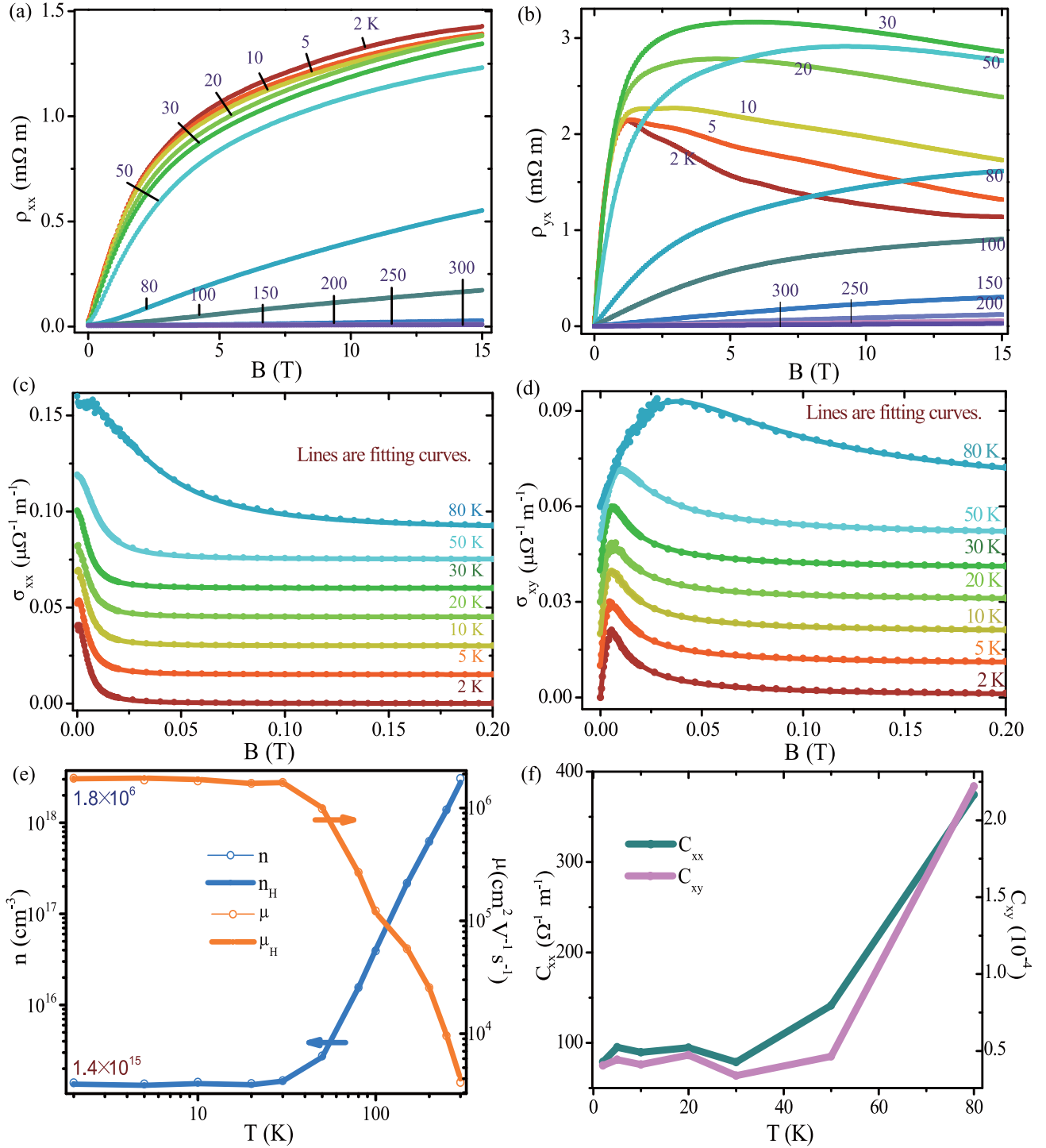


FIG. 3. Measured longitudinal resistivity (a) and Hall resistivity (b) of sample 3 (s3). (c) and (d) Corresponding conductivity tensors. Dots are experimental results and lines are fitting curves in a two-carrier model. (e) Temperature dependence of the carrier density and mobility of the dominated carriers, estimated from analyses for the conductivity tensors independently. (f) Fitting parameters C_{xx} and C_{xy} at low temperatures.

provides a strong evidence for the chiral anomaly mechanism. The estimated C_w from fitting is monotonically decreasing from 0.014 ± 0.001 at 2 K to $0.002 \pm (<0.001)$ at 50 K [34], revealing a reasonable temperature dependence of the chiral anomaly.

To further understand the properties of HfTe $_5$, Hall effect is studied in sample 3 (s3) as shown in Fig. 3. Figure 3(a) shows the magnetoresistivity ρ_{xx} at selected temperatures under an external perpendicular magnetic field ($B//b$ axis). The positive magnetoresistivity at 2 K is as large as 6000%

in an applied field of 15 T. Even at room temperature 300 K, the value of $\rho(15\text{ T})/\rho(0\text{ T})$ is about 150%. Hall resistivity $\rho_{yx}(V_{yx}/I)$ of HfTe₅ crystal is shown in Fig. 3(b) and positive Hall coefficient is observed. At the base temperature 2 K, ρ_{yx} first increases and then decreases with the increasing magnetic field. The decreasing behavior is weakened by the increased temperatures. At a temperature above 80 K, we observe a monotonically increased ρ_{yx} curve with changing slope in magnetic field up to 15 T.

With the measured ρ_{xx} and ρ_{yx} , we show the longitudinal conductivities σ_{xx} and Hall conductivities σ_{xy} of s3 in Figs. 3(c) and 3(d), respectively. The curves at temperatures

above 2 K are shifted for clarity. In a two-carrier model, σ_{xx} and σ_{xy} data are fitted with the following formula [35]:

$$\sigma_{xx} = \frac{ne\mu}{1 + (\mu B)^2} + C_{xx}, \quad (2)$$

$$\sigma_{xy} = n_H e \mu_H^2 B \left[\frac{1}{1 + (\mu_H B)^2} + C_{xy} \right]. \quad (3)$$

Here $n(n_H)$ and $\mu(\mu_H)$ is the density and mobility for the high-mobility carriers deduced from $\sigma_{xx}(\sigma_{xy})$, respectively. $C_{xx}(C_{xy})$ denotes the low-mobility components estimated from $\sigma_{xx}(\sigma_{xy})$. In Figs. 3(c) and 3(d), fitting lines show

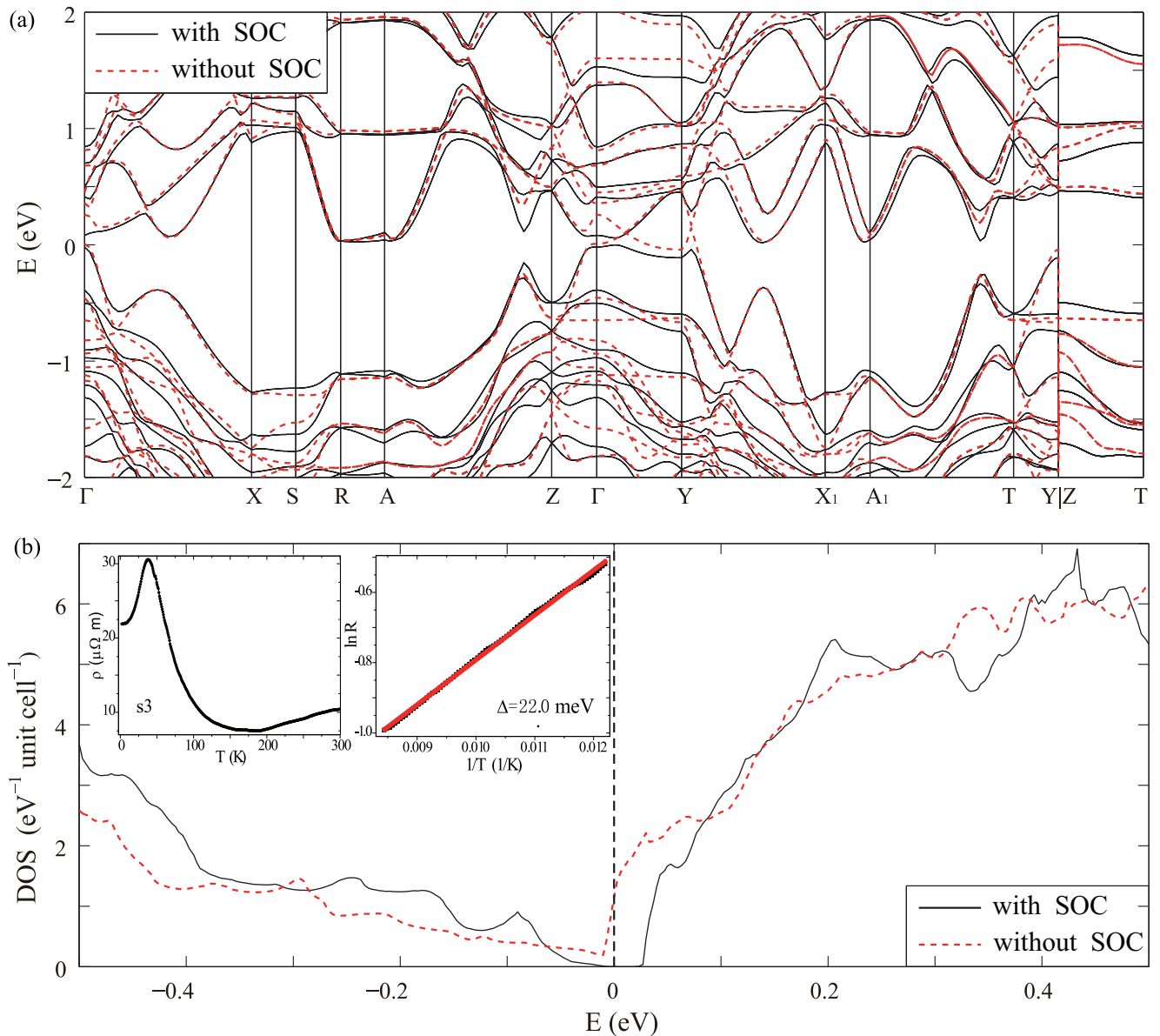


FIG. 4. (a) The calculated band structure of HfTe₅ with (black solid curves) and without (red dashed curve) spin-orbit coupling (SOC). The Brillouin zone path is chosen as the same with [39]. The Fermi energy is shifted to 0 eV. (b) The calculated density of states (DOS) of HfTe₅ with (black solid curve) and without (red dashed curve) SOC. Both the band structure and DOS results indicate an SOC-induced semimetal-insulator transition. Left inset shows the resistance vs temperature curve of s3. The peak anomaly may be due to the competition between the metallic surface states and thermal excitations from bulk states. Right inset shows a $\ln R$ vs $1/T$ plot in the temperature range from 82 to 125 K for the same sample. The black dots are experimental data and the red line is a linear fitting curve. This allows us to extract a gap ~ 22.0 meV through $\ln R \sim \Delta/2k_B T$, close to the calculated value of 18.4 meV.

excellent agreement with the experimental dots. Fitting parameters as a function of temperature are shown in Figs. 3(e) and 3(f) [34]. We can see from Fig. 3(e) the carrier density n and n_H agrees very well with each other, though they are obtained from the analyses of σ_{xx} and σ_{xy} independently. The mobility μ and μ_H also coincide perfectly, which verifies the validity of our analyses within the two-carrier model. C_{xx} and C_{xy} related to the low-mobility carriers are displayed in Fig. 3(f). We analyze the low mobility carrier and deduce the respective μ_L from C_{xx} and C_{xy} , which satisfies $(\mu_L \mathbf{B})^2 \ll 1$ in our fitting regime from 0 to 0.2 T for temperatures below 80 K, justifying the applicability of Eqs. (2) and (3).

As shown in Fig. 3(e), the carrier density of HfTe₅ at 2 K is estimated to be $n = 1.40 \pm 0.006 \times 10^{15}/\text{cm}^3$ ($n_H = 1.35 \pm 0.006 \times 10^{15}/\text{cm}^3$). This maps a very small Fermi surface, as estimated in previous study [24,25]. As the temperature is increased, the carrier density grows slightly and shows a clear increase above 100 K. Besides, the mobility of the dominant carriers in HfTe₅ is decreasing with increasing temperature. At 2 K, the mobility is remarkably high as $\mu = 1.84 \pm 0.01 \times 10^6 \text{ cm}^2 \text{ V}^{-1} \text{ s}^{-1}$ ($\mu_H = 1.82 \pm 0.01 \times 10^6 \text{ cm}^2 \text{ V}^{-1} \text{ s}^{-1}$), comparable to that of Dirac/Weyl fermions in Cd₃As₂ [9,32] and TaAs family [10–15]. It is worth noting that this is about two orders of magnitude higher than that of ZrTe₅ [29]. Even at room temperature, the mobility of our HfTe₅ crystal is as high as $3700 \text{ cm}^2 \text{ V}^{-1} \text{ s}^{-1}$, which is significant for the potential electronic applications.

As described above, ZrTe₅ has been examined by the ARPES result, magneto-optical spectroscopy, and magneto-transport measurements [13,28,29]. The nontrivial topological properties of ZrTe₅ have been revealed. We know that the crystalline structure and energy band structure of HfTe₅ resemble those of ZrTe₅. From the Hall traces and two-carrier model analyses, we find that hole type carriers dominate the electrical transport in our HfTe₅ samples. The single type hole carrier is consistent with the previously calculated band structures in Ref. [27], in which the carrier type is either electron or hole for a given Fermi level. Our transport measurements have demonstrated that the distinct chiral anomaly originates from the topological property of HfTe₅, which is similar to that in Na₃Bi and Cd₃As₂ systems [8,17,18].

The experimental results are fully consistent with the 3D Dirac semimetal scenario, with finite Fermi surface. It may be remarked that observed quantum chiral anomaly in the transport measurements with a finite Fermi surface does not shed light on the existence of a quasiparticle gap at very low energy. We therefore examine the question of gaplessness of truly low-energy excitations, which is not protected by symmetry anyway, using band structure calculation. The first-principles calculation is performed with the VASP package [36]. The projector-augmented wave pseudopotentials are employed with the Perdew-Burke-Ernzerhof exchange-correlation functional. The plane-wave energy cut-off is 330 eV and the Brillouin zone is sampled with an $11 \times 11 \times 7$ grid. The lattice is relaxed with a force threshold of 0.01 eV/Å and with the optB86b functional [37,38] in order to take into account the van der Waals interaction.

Our first-principles calculation shows that HfTe₅ is a small gap topological insulator. The results are summarized in

Fig. 4. The band structure without spin-orbit coupling (SOC) indicates that HfTe₅ is a semimetal. However, when the SOC is included, the low-energy spectrum becomes fully gapped with an indirect gap of 18.4 meV, as indicated both from the band structure and density of states. The computed band gap is comparable to the exponential fitting of the ρ - T curve in the region of intermediate temperature, as shown in the insets of Fig. 4(b). The resistance peak may come from the competition of its surface metallic states and thermally induced carriers in the insulating bulk. We have also calculated the Z_2 topological invariant, and the result shows that it is a 3D strong topological insulator for both the relaxed structure and the experimental structure. The coexistence of bulk states and surface states may also lend support to the validity of the two-carrier model analysis of the Hall measurement. The consistency between experimental results and computed band structure with a gap therefore leads us to discuss the interesting possibility of chiral anomaly in a small gap topological insulator. As justified in Ref. [6], the chiral symmetry is always approximate in lattice systems due to the mass term, and the magnetic field induced chiral anomaly exists only when the chiral charge relaxation time τ_a greatly exceeds the mean free time τ_0 . Thus, in topological insulators with small energy gap and high Fermi energy, the characteristic time τ_a can also be much larger than τ_0 , which leads to the chiral anomaly observed in HfTe₅ samples. This argument is valid, with or without a band gap, and in the event the system is driven to a weak topological insulator via further band inversion by, for example, strain or lattice relaxation.

III. CONCLUSIONS

In summary, by performing systematic electrical transport measurements, we first observed the evidence for chiral anomaly and ultrahigh mobility in HfTe₅ crystals. Particularly, an anomalous negative magnetoresistivity is observable when the magnetic field \mathbf{B} and electrical field \mathbf{E} are aligned parallel. It is most evident when \mathbf{B}/\mathbf{E} and sensitive to the orientation of \mathbf{B} relative to \mathbf{E} . Our quantitative analyses identify the chiral anomaly as the underlying origin of negative magnetoresistivity. Furthermore, we find HfTe₅ has ultrahigh mobility and ultralow carrier density by analyzing both the longitudinal and Hall conductivities in a two-carrier model, indicating potential application in electronics.

Note added: We note that another group has also experimentally studied the transport properties of HfTe₅ [40].

ACKNOWLEDGMENTS

We acknowledge Yongjie Liu for the help in the pulsed magnetic field measurements and we thank Honglie Ning for valuable discussions. This work was financially supported by the National Basic Research Program of China (Grants No. 2013CB934600, No. 2012CB921300, and No. 2013CB921900), and the Open Project Program of the Pulsed High Magnetic Field Facility (Grant No. PHMFF2015002), Huazhong University of Science and Technology. D.G.M and J.-Q.Y acknowledge support from NSF DMR 1410428.

Huichao Wang and Chao-Kai Li contributed equally to this work.

- [1] S. Adler, *Phys. Rev.* **177**, 2426 (1969).
- [2] J. S. Bell and R. Jackiw, *Nuovo Cim. A* **60**, 47 (1969).
- [3] H. B. Nielsen and M. Ninomiya, *Phys. Lett. B* **130**, 389 (1983).
- [4] D. T. Son and B. Z. Spivak, *Phys. Rev. B* **88**, 104412 (2013).
- [5] A. A. Burkov, *J. Phys. Condens. Matter* **27**, 113201 (2015).
- [6] A. A. Burkov, *Phys. Rev. B* **91**, 245157 (2015).
- [7] H.-J. Kim, K.-S. Kim, J.-F. Wang, M. Sasaki, N. Satoh, A. Ohnishi, M. Kitaura, M. Yang, and L. Li, *Phys. Rev. Lett.* **111**, 246603 (2013).
- [8] J. Xiong, S. K. Kushwaha, T. Liang, J. W. Krizan, M. Hirschberger, W. D. Wang, R. J. Cava, and N. P. Ong, *Science* **350**, 413 (2015).
- [9] T. Liang, Q. Gibson, M. N. Ali, M. Liu, R. J. Cava, and N. P. Ong, *Nat. Mater.* **14**, 280 (2015).
- [10] X. C. Huang, L. X. Zhao, Y. J. Long, P. P. Wang, D. Chen, Z. H. Yang, H. Liang, M. Q. Xue, H. M. Weng, Z. Fang, X. Dai, and G. F. Chen, *Phys. Rev. X* **5**, 031023 (2015).
- [11] C. L. Zhang, S.-Y. Xu, I. Belopolski, Z. J. Yuan, Z. Q. Lin, B. B. Tong, G. Bian, N. Alidoust, C.-C. Lee, S.-M. Huang, T.-R. Chang, G. Q. Chang, C.-H. Hsu, H.-T. Jeng, M. Neupane, D. S. Sanchez, H. Zheng, J. F. Wang, H. Lin, C. Zhang, H.-Z. Lu, S.-Q. Shen, T. Neupert, M. Z. Hasan, and S. Jia, *Nat. Commun.* **7**, 10735 (2016).
- [12] C. Shekhar, A. K. Nayak, Y. Sun, M. Schmidt, M. Nicklas, I. Leermakers, U. Zeitler, Y. Skourski, J. Wosnitzer, Z. K. Liu, Y. L. Chen, W. Schnelle, H. Borrmann, Y. Grin, C. Felser, and B. H. Yan, *Nat. Phys.* **11**, 645 (2015).
- [13] Q. Li, D. E. Kharzeev, C. Zhang, Y. Huang, I. Pletikosić, A. V. Fedorov, R. D. Zhong, J. A. Schneeloch, G. D. Gu, and T. Valla, *Nat. Phys.* (2016), doi:[10.1038/nphys3648](https://doi.org/10.1038/nphys3648).
- [14] X. J. Yang, Y. P. Li, Z. Wang, Y. Zheng, and Z.-A. Xu, [arXiv:1506.03190](https://arxiv.org/abs/1506.03190).
- [15] C. L. Zhang, C. Guo, H. Lu, X. Zhang, Z. J. Yuan, Z. Q. Lin, J. F. Wang, and S. Jia, *Phys. Rev. B* **92**, 041203(R) (2015).
- [16] C. Zhang, E. Z. Zhang, Y. W. Liu, Z.-G. Chen, S.H. Liang, J. Z. Cao, X. Yuan, L. Tang, Q. Li, T. Gu, Y. Z. Wu, J. Zou, and F. X. Xiu, [arXiv:1504.07698](https://arxiv.org/abs/1504.07698).
- [17] C.-Z. Li, L.-X. Wang, H. W. Liu, J. Wang, Z.-M. Liao, and D.-P. Yu, *Nat. Commun.* **6**, 10137 (2015).
- [18] H. Li, H. T. He, H.-Z. Lu, H. C. Zhang, H. C. Liu, R. Ma, Z. Y. Fan, S.-Q. Shen, and J. N. Wang, *Nat. Commun.* **7**, 10301 (2016).
- [19] I. M. Tsidilkovskii, W. Giriat, G. I. Kharus, and E. A. Neifeld, *Phys. Status Solidi B* **64**, 717 (1974).
- [20] N. Kikugawa, P. Goswami, A. Kiswandhi, E. S. Choi, D. Graf, R. E. Baumbach, J. S. Brooks, K. Sugii, Y. Iida, M. Nishio, S. Uji, T. Terashima, P. M. C. Rourke, N. E. Hussey, H. Takatsu, S. Yonezawa, Y. Maeno, and L. Balicas, *Nat. Commun.* **7**, 10903 (2016).
- [21] S. Furuseth, L. Brattas, and A. Kjekshus, *Acta. Chem. Scand.* **27**, 2367 (1973).
- [22] M. Izumi, K. Uchinokura, and E. Matsuura, *Solid State Commun.* **37**, 641 (1981).
- [23] T. M. Tritt, N. D. Lowhorn, R. T. Littleton, A. Pope, C. R. Feger, and J. W. Kolis, *Phys. Rev. B* **60**, 7816 (1999).
- [24] R. Shaviv, E. F. Westrum, Jr., H. Fjellvag, and A. Kjekshus, *J. Solid State Chem.* **81**, 103 (1989).
- [25] G. N. Kamm, D. J. Gillespie, A. C. Ehrlich, D. L. Peebles, and F. Levy, *Phys. Rev. B* **35**, 1223 (1987).
- [26] M. Izumi, T. Nakayama, K. Uchinokura, S. Harada, R. Yoshizaki, and E. Matsuura, *J. Phys. C: Solid State Phys.* **20**, 3691 (1987).
- [27] H. M. Weng, X. Dai, and Z. Fang, *Phys. Rev. X* **4**, 011002 (2014).
- [28] R. Y. Chen, Z. G. Chen, X.-Y. Song, J. A. Schneeloch, G. D. Gu, F. Wang, and N. L. Wang, *Phys. Rev. Lett.* **115**, 176404 (2015).
- [29] X. Yuan, C. Zhang, Y. W. Liu, C. Y. Song, S. D. Shen, X. Sui, J. Xu, H. C. Yu, Z. H. An, J. Zhao, H. G. Yan, and F. X. Xiu, [arXiv:1510.00907](https://arxiv.org/abs/1510.00907).
- [30] P. C. Canfield, T. Kong, U. S. Kaluarachchi, and N. H. Jo, *Philos. Mag.* **96**, 84 (2016).
- [31] M. N. Ali, L. Schoop, J. Xiong, S. Flynn, Q. Gibson, M. Hirschberger, N. P. Ong, and R. J. Cava, *Europhys. Lett.* **110**, 67002 (2015).
- [32] Y. F. Zhao, H. W. Liu, C. L. Zhang, H. C. Wang, J. F. Wang, Z. Q. Lin, Y. X., H. Lu, J. Liu, Y. Wang, S. M. Brombosz, Z. L. Xiao, S. Jia, X. C. Xie, and J. Wang, *Phys. Rev. X* **5**, 031037 (2015).
- [33] J. Y. Feng, Y. Pang, D. S. Wu, Z. J. Wang, H. M. Weng, J. Q. Li, Z. Fang, Y. G. Shi, and L. Lu, *Phys. Rev. B* **92**, 081306 (2015).
- [34] See Supplemental Material at <http://link.aps.org/supplemental/10.1103/PhysRevB.93.165127> for detailed fitting parameters.
- [35] H. Takahashi, R. Okazaki, Y. Yasui, and I. Terasaki, *Phys. Rev. B* **84**, 205215 (2011).
- [36] G. Kresse and J. Furthmüller, *Phys. Rev. B* **54**, 11169 (1996).
- [37] J. Klimeš, D. R. Bowler, and A. Michaelides, *J. Phys.: Condens. Matter* **22**, 022201 (2010).
- [38] J. Klimeš, D. R. Bowler, and A. Michaelides, *Phys. Rev. B* **83**, 195131 (2011).
- [39] W. Setyawan and S. Curtarolo, *Comput. Mater. Sci.* **49**, 299 (2010).
- [40] L. X. Zhao, X. C. Huang, Y. J. Long, D. Chen, H. Liang, Z. H. Yang, M. Q. Xue, Z. A. Ren, H. M. Weng, Z. Fang, X. Dai, and G. F. Chen, [arXiv:1512.07360](https://arxiv.org/abs/1512.07360).